JOURNAL OF MATERIALS SCIENCE 27 (1992) 5229–5238

Influence of calcination, sintering and composition upon microwave properties of the $Ba_{6-x}Sm_{8+2x/3}Ti_{18}O_{54}$-type oxide

P. LAFFEZ, G. DESGARDIN, B. RAVEAU
CRISMAT-ISMRa, Boulevard du Maréchal Juin, 14050 Caen Cedex, France

Dielectric ceramic compositions for microwave applications belonging to the (BaO) (Sm_2O_3) (TiO_2) ternary phase diagram were studied. Calcination, sintering, microwave properties and influence of secondary phases were investigated. By varying composition and/or sintering process, a high dielectric constant with low dielectric losses and modulable negative or positive temperature coefficient of the resonant frequency can be reach.

1. Introduction

Dielectric ceramics for resonators are of great interest because they will probably be used to manufacture pass-band filters for microwave applications. Three parameters, dielectric constant, ε, quality factor, Q, and the temperature coefficient of resonant frequency, τf must be carefully controlled for such applications. The ε value dictates the volume of the resonator which varies as $\varepsilon^{1/2}$, and is expected to have an average value of 80. The quality factor, Q, which is the inverse of the loss angle, tg (tangent) δ, corresponds approximatively to a constant Qf product, f being the frequency. The temperature coefficient, $\tau f = 1/f(df/dt)$, is practically always required to be as close as possible to zero.

Many systems have been investigated for the research of new materials, but only a limited number lead to interesting characteristics. Among them, the pseudo ternary systems $BaO–Ln_2O_3–TiO_2$ with Ln = Sm or Nd, appear as potential candidates [1, 2]. Similarly, the partial replacement of barium by strontium or lead in these systems was studied [1–3]. The best results were obtained for the composition $(BaO)_{0.15}(Sm_2O_3)_{0.15}(TiO_2)_{0.7}$ by Nishigaki *et al.* [1], with a partial substitution of barium by strontium. However, for this composition, the authors obtained a mixture of the main phase belonging to the $Ba_{6-x}Sm_{8+2x/3}Ti_{18}O_{54}$-type structure [4] and of secondary phases TiO_2 and $Ba_2Ti_9O_{20}$. Moreover, the authors point out that the degradation of radio-frequency properties of this ceramic is due to the secondary phases. The possible nonstoichiometry ($0 \leq x \leq 1.5$ for samarium) of the main phase [4], which exhibits a tunnel structure related to the tungsten bronzes A_xWO_3, suggests that the reaction mechanisms which take place during sintering in this system are complex. The present paper reports a study of the influence of calcination and sintering conditions upon microwave properties of the compositions close to the ideal pure phase bronzoid $Ba_{6-x}Sm_{8+2x/3}Ti_{18}O_{54}$.

2. Experimental procedure

2.1. Sample preparation

Adequate mixtures of $BaCO_3$, Sm_2O_3 and TiO_2 were intimately ground by attrition in a teflon bowl using deionized water and zirconia balls. The mixed raw material was then dried under an infrared radiator at 400 °C. The resulting powder was ground by hand and screened with 100 μm meshes, to eliminate agglomerates, and calcined at different temperatures in alumina boats. Calcination was followed by a second attrition-grinding in order to reach an homogeneous granulometric distribution, close to 1 μm.

The powders were then added to an organic binder (Rhodoviol 5%) and pressed in the form of cylinders using an uniaxial pneumatic press, and finally sintered at high temperature in a tubular furnace.

2.2. Characterization

The calcined and sintered samples were characterized by X-ray diffraction (XRD) using a Guinier camera and a powder diffractometer. Fractures and polished areas of the sintered samples were observed by scanning electron microscopy using a Jeol 840 Microscop equipped with Tracor analysis. For this purpose, thermal treatment at 1150 °C for 5 min allowed grain boundaries to be revealed. The reactivity and sintering phenomena were studied by differential thermal analyses (DTA), thermogravimetry (TG) and dilatometric techniques.

Microwave characteristics were determined by the Tekelec Microwave Society (Montreuil 93106, France) using a dielectric resonator method previously described [5].

3. Results and discussion

3.1. The optimized composition $(BaO)_{0.15}$ $(Sm_2O_3)_{0.15}$ $(TiO_2)_{0.7}$

This composition, "a" in Fig. 1, was chosen owing to its good microwave properties previously published [1].

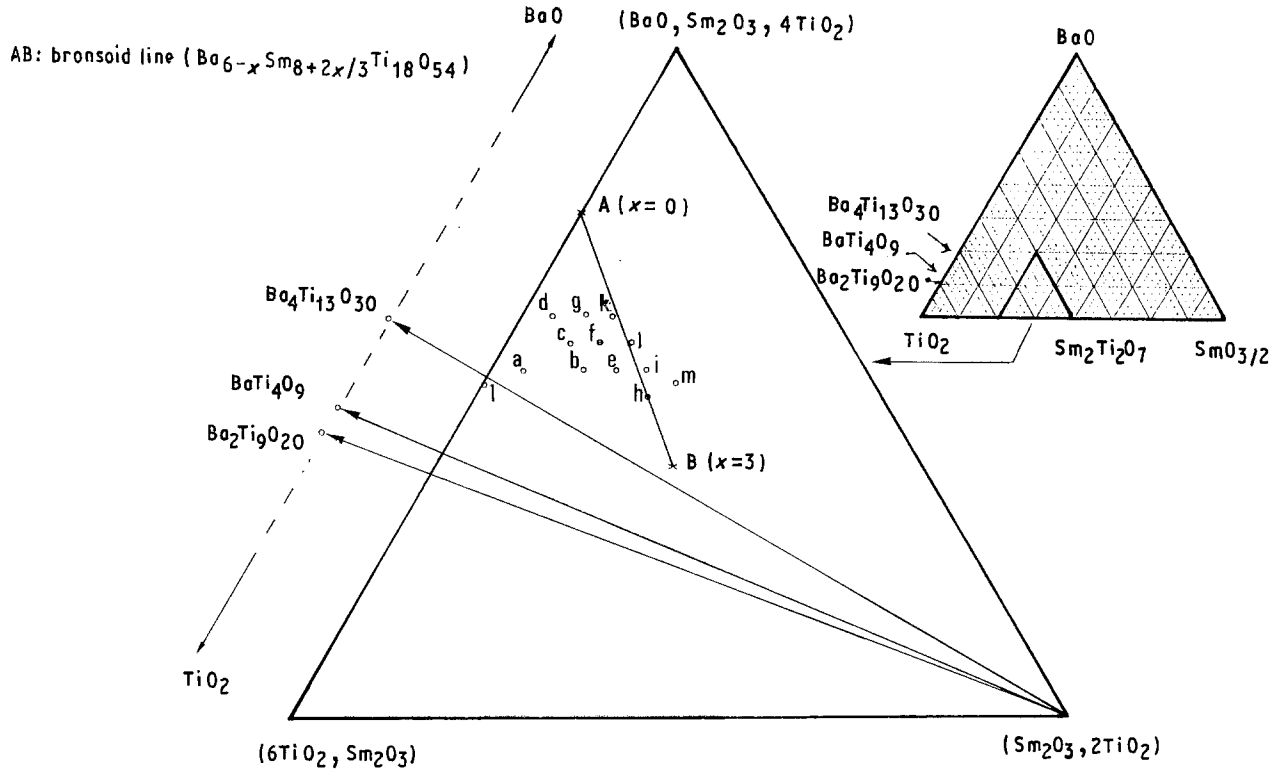

Figure 1 Part of the ternary diagram (BaO) ($SmO_{3/2}$) (TiO_2).

3.1.1. Calcination and microwave properties

X-ray diffraction analysis show that the phases $BaTi_4O_9$, $Sm_2Ti_2O_7$ and $Ba_4Ti_{13}O_{40}$ are formed in a first step (Table I). The expected bronzoid, corresponding to the ideal formula $Ba_{6-x}Sm_{8+2x/3}Ti_{18}O_{54}$ [4], appears only at 1000 °C; it coexists with small amounts of $Sm_2Ti_2O_7$ at high temperature (1200 °C). The ternary diagram (Fig. 1) shows that for temperatures smaller than 1100 °C, the mixture of three phases which is obtained is in agreement with the homogeneity range of the bronzoid represented by the line AB in Fig. 1. On the other hand, for higher temperatures it suggests that the bronzoid and $Sm_2Ti_2O_7$ are not the only phases which are present in the mixture, but that a third phase exists, for instance TiO_2, which is in too small amounts to be detected by XRD. The SEM observations on sintered materials support this view.

These results, although rather similar to those recently observed by Wu and Chang [6], exhibit some differences. With our experimental method, the formation of the nonstoichiometric tunnel structure is observed at 1000 °C instead of at 1050 °C by previous authors [6]. This is easily explained by our milling process and calcination which allows a different reactivity of the powder to be reached. The latter hypothesis is confirmed by the fact that in our case at 1000 °C, $BaTi_4O_9$ has completely disappeared contrary to what was found by Wu and Chang [6] at the same temperature.

TABLE I Phase evolution during calcination of $0.15BaCO_3 + 0.15Sm_2O_3 + 0.7TiO_2$ (composition 'a')

Calcination temperature (°C)	Detected phases
950	TiO_2(w) Sm_2O_3(S), $BaTiO_4O_9$(m), $Ba_4Ti_{13}O_{30}$(m), $Sm_2Ti_2O_7$(s)
1000	$Ba_4Ti_{13}O_{30}$(m), $Sm_2Ti_2O_7$(s), ϕ(w)
1050	$Ba_4Ti_{13}O_{30}$(m), $Sm_2Ti_2O_7$(s), ϕ(m)
1100	$Ba_4Ti_{13}O_{30}$(w), $Sm_2Ti_2O_7$(s), ϕ(s)
1150	$Sm_2Ti_2O_7$(w), ϕ(s)
1200	$Sm_2Ti_2O_7$(w), ϕ(s)

ϕ, Bronzoid $Ba_{6-x}Sm_{8+2x/3}Ti_{18}O_{54}$; (w), weak; (m), medium; (s), strong.

The TG analysis performed in air confirms the early decomposition of $BaCO_3$ (Fig. 2a) at 900 °C. This allows a low temperature of calcination to be used in order to eliminate CO_2. DTA (Fig. 3a), shows a broad exothermic signal ranging from 900–1200 °C, evidence of the complex reaction mechanisms involved in the formation of the bronzoid $Ba_{6-x}Sm_{8+2x/3}Ti_{18}O_{54}$.

Although at 900 °C, CO_2 gas has been eliminated, the calcination temperature is liable to influence microwave characteristics after sintering. Thus, a series of calcinations were performed at different temperatures, and the corresponding samples were all sintered under the same conditions, i.e. at 1350 °C for 2 h in air. Table II shows that the microwave properties are almost independent of temperature except at 1100 °C. At this temperature, a relatively low but significant degradation of the microwave characteristics is observed. This phenomenon already reported by Wu and Chang [6] was attributed to a variation of the TiO_2 amount, present in the matrix as a secondary phase. We were unable to confirm their interpretation from our own SEM observations. Neither TGA and DTA, nor XRD studies allowed any anomaly with respect to other temperatures of calcination to be detected.

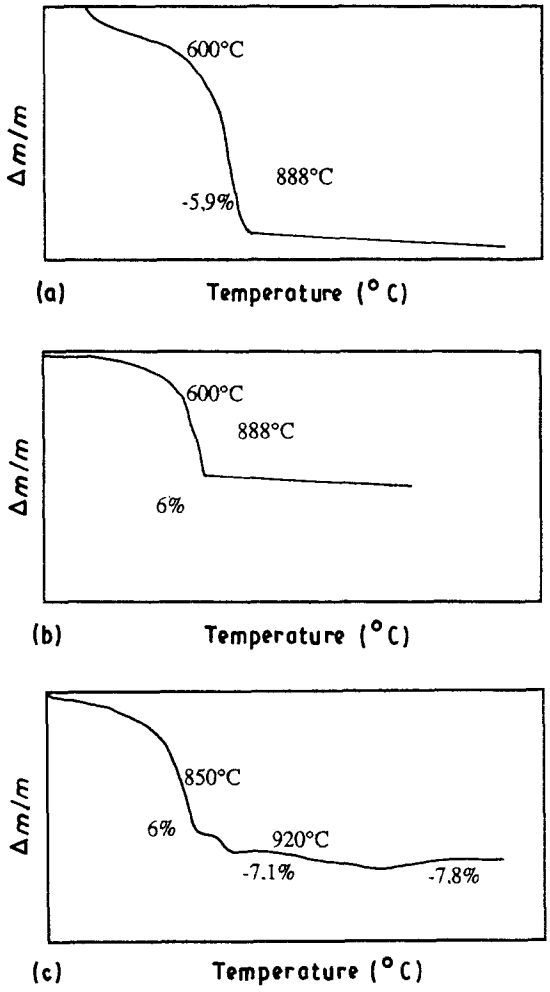

Figure 2 TG of composition 'a' in (a) air, (b) oxygen and (c) argon atmosphere.

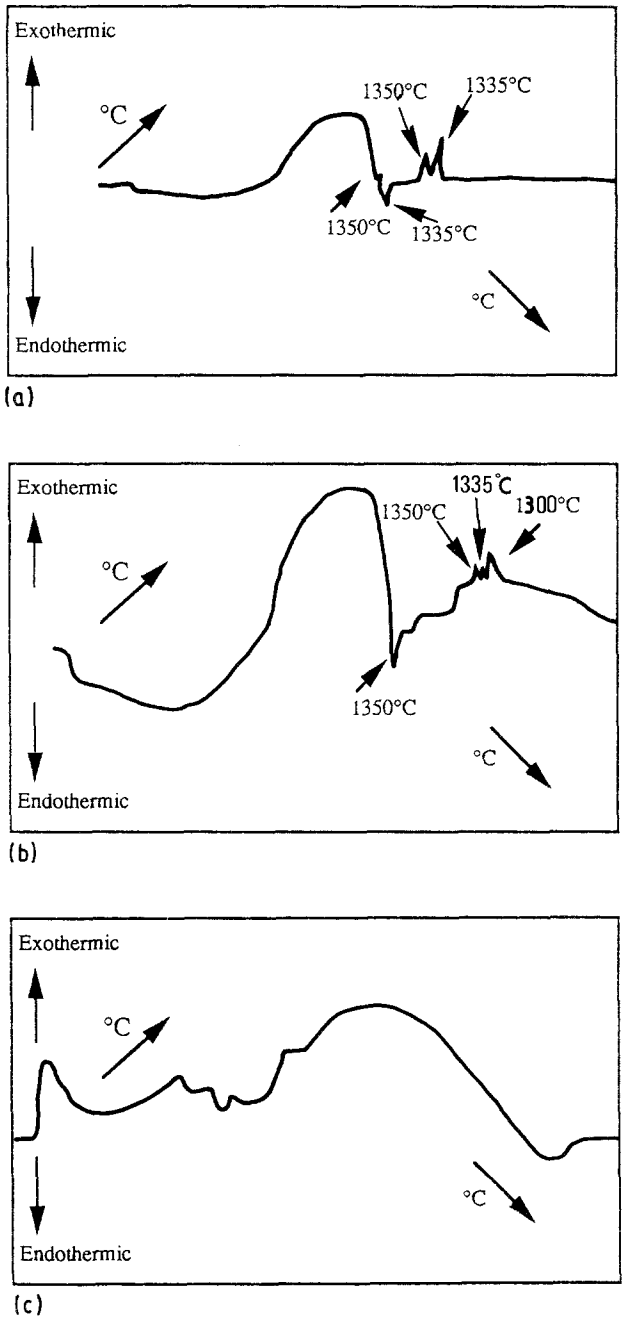

Figure 3 DTA of the composition 'a' in (a) air, (b) oxygen and (c) argon atmospheres.

3.1.2. Sintering and microwave properties

The evolution of the shrinkage in air for a pellet of powder calcined at 950 °C and using a heating rate of 200 °C h^{-1} is shown in Fig. 4a. After the usual dilatation until 700 °C, we observed a bending of the curve until 1000 °C, corresponding to the formation of $Sm_2Ti_2O_7$. The second dilatation observed between 1000 and 1050 °C corresponds to the formation of the bronzoid $Ba_{6-x}Sm_{8+2x/3}Ti_{18}O_{54}$. The shrinkage begins at 1150 °C; it accelerates quickly and becomes maximum at about 1300 °C, stopping at 1320–1360 °C. Beyond this temperature the shrinkage starts again and carries on during the plateau at 1400 °C (60 min). Then, an anomaly is observed during cooling from 1400 °C to 1380 °C: the shrinkage carries on and suddenly a large dilatation corresponding to two steps is observed around 1335 °C. These two anomalies can be correlated to the DTA in air (Fig. 2a) which shows two endothermic peaks, at 1335 and 1350 °C, as temperature increases; moreover, it must be pointed out that these transformations are reversible, because two exothermic peaks are observed when the temperature is decreased.

The dilatometric study in an oxygen flow (Fig. 4b) leads to a similar dilatometric curve up to 700 °C. At this temperature there is no slowing down of dilatation, as in air. Shrinkage starts earlier; i.e. at 1100 °C; this demonstrates the effect of oxygen pressure upon the kinetics of sintering. At higher temperature, one observes the same general behaviour as in air; during cooling dilatation has a much higher amplitude and corresponds to only one step. It is also worth pointing out that the final shrinkage is 6% larger in an oxygen flow than in air. The DTA study performed in an

TABLE II Microwave characteristics versus calcination temperature of composition 'a', sintered at 1350 °C, 2 h in an air atmosphere

Calcination temperature (°C)	Density	ε	Qf (GHz)	τf (p.p.m. °C^{-1})
950	5.59	75	8670	0
1000	5.58	75	8600	0
1100	5.46	73	8200	+ 3
1150	5.55	75	8600	0
1200	5.53	75	8700	0

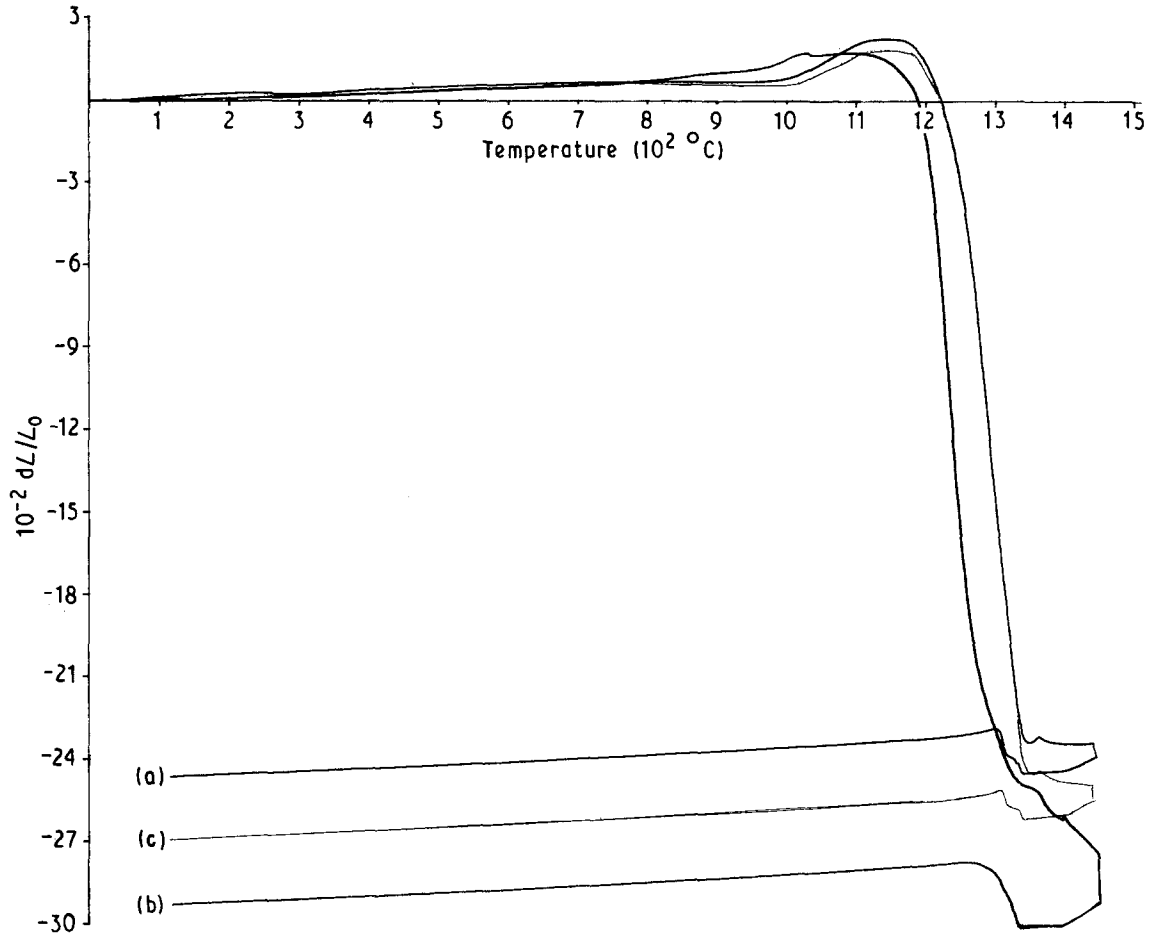

Figure 4 Shrinkage evolution of a pellet of composition 'a' calcinated at 950 °C in (a) air, (b) oxygen and (c) argon flow.

oxygen flow shows a similar behaviour to that observed in air (Fig. 3b); nevertheless, an additional peak appears at 1300 °C, which is especially visible when temperature decreases.

The dilatometric curve obtained in an argon flow is very similar to that observed in air (Fig. 4c), with a higher final shrinkage. Curiously the corresponding DTA curve does not exhibit any peak at high temperature (Fig. 3c).

This suggests that the DTA peaks should correspond to oxygen absorption or desorption during sintering. TGA is in agreement with this view point: above 900 °C the TG curve of the argon-treated sample exhibits a new loss of weight (Fig. 1c) with respect to the samples studied in air (Fig. 1a) or oxygen (Fig. 1b). Thus the final loss of weight is 2% greater in argon with respect to oxygen or air.

However, as stated previously, the studied composition does not correspond to pure bronzoid. This suggest that the DTA peaks could also be correlated with the transformations which can be deduced from the (BaO, TiO_2) phase diagram established by O'Brian and Thomson [7]. In particular, these authors point out two titanates $Ba_4Ti_{13}O_{30}$ and $Ba_6Ti_{17}O_{40}$ which melt incongruently at 1366 and 1346 °C, respectively. The discordance between O'Brian and Thomson's results and our DTA peaks could be due to the rapid kinetics and the uncertainty in the temperature determination. These remarks are in agreement with the interpretation of the dilatometric curves which points out in each case an incident at 1365 °C when increasing temperature and a large dilatation below 1335 °C during cooling.

From these observations one can postulate the presence of $Ba_4Ti_{13}O_{30}$ and probably $Ba_6Ti_{17}O_{40}$ as secondary phases beside the bronzoid.

These phenomena require further investigations for a complete understanding of the shrinkage mechanism; nevertheless these results allowed us to choose the sintering temperatures in the range 1350–1380 °C.

3.1.3. Microstructure evolution with sintering temperature

Fig. 5 shows microstructures of ceramics sintered at 1350 °C under an air flow. All show a polyphase material with at least two secondary phases. XRD and EDS analysis have been performed in order to identify these secondary phases. The XRD pattern is very difficult to interpret because of the overlapping of the main lines of the different possible titanates and of the small amount of the secondary phases; however, two secondary phases, i.e. TiO_2 and $Ba_2Ti_9O_{20}$ as previously reported [1] can be detected unambiguosly. The $Ba_4Ti_{13}O_{30}$ phase, postulated in the previous paragraph, is not visible on the X-ray pattern. However, this phase was detected during calcination. It transforms during sintering but a small amount can remain undetected by X-ray diffraction. The EDS analysis confirms the presence of TiO_2 and $Ba_2Ti_9O_{20}$ as major secondary phases.

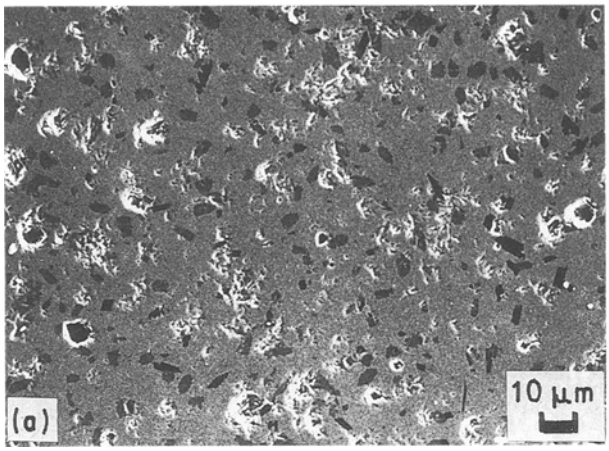

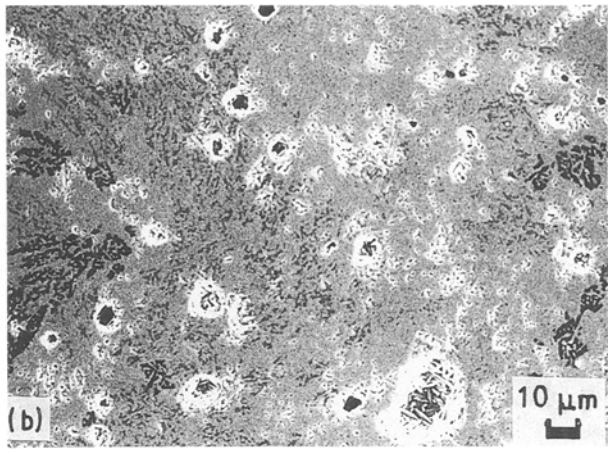

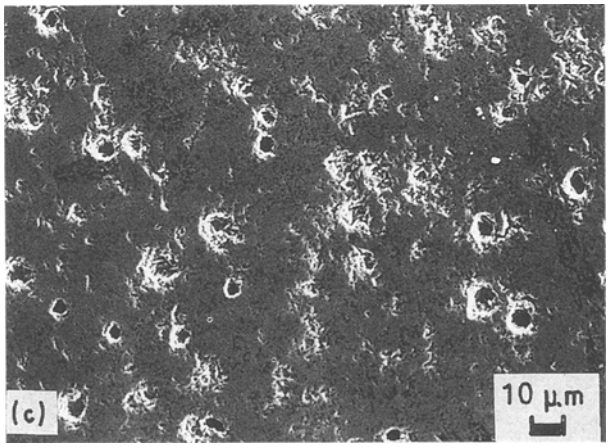

Figure 5 Microstructure evolution of a pellet of composition 'a' calcinated at 950 °C and sintered at (a) 1350 °C, (b) 1360 °C and (c) 1370 °C under an air flow.

In addition, microstructures show that when the sintering temperature increases, the statistically distributed second phases observed at temperatures lower than 1350 °C disappears, leading to the formations of aggregates when the temperature reaches 1360 or 1370 °C. At the same time, the crystal growth hinders the pore migration towards the surface area leading to a secondary porosity decreasing the bulk density (Table III).

3.1.4. Improvement of the density by Fe_2O_3 doping

Several attempts at grinding with an attritor by substituting zirconia balls with iron balls allowed a lower porosity of the final ceramic to be reached. Atomic absorption analysis of the corresponding samples showed Fe contents of 700 p.p.m. A systematic study of the influence of Fe_2O_3 doping was undertaken using zirconia balls for milling. It was observed that porosity decreases on the addition of Fe_2O_3, and that pores tend to accumulate. An optimum compacity is reached for a content of 200 p.p.m. Fe_2O_3, as shown in Fig. 6, where the porosity is practically eliminated. An increase of Fe_2O_3 content again induces unequally dispersed porosity.

TABLE III Atmospheric influence on microwave properties of composition 'a' ceramic sintered at 1350 °C and calcined at 950 °C

Atmosphere	Density	ε	Qf(GHz)	τf(p.p.m. °C^{-1})
Air	5.45–5.6	73–75	8600–9000	− 3 to 0
O_2	5.6	77–78	8900–9000	− 6 to 3

3.1.5. Microwave characteristics

In order to test the influence of sintering temperature upon microwave properties, different temperatures have been used between 1350 and 1380°C, according to a dilatometric study. Table III shows the degradation of microwave characteristics as soon as the sintering temperature is greater than 1350 °C. The dielectric constant decreases and τf increases. One can easily explain the ε decrease by the decrease in bulk density according to microstructure observations and dilatometric results.

The sintering atmosphere does not dramatically influence the microwave characteristics (Table IV). Nevertheless, a significant improvement of ε is observed from 73–75 to 77–78 and a decrease of τf from − 3 p.p.m. °C^{-1} to − 6 p.p.m °C^{-1} when the samples are sintered in an oxygen flow instead of air.

The variation of the microwave characteristics with the Fe_2O_3 content of doped samples (Table V) shows that up to 200 p.p.m. Fe_2O_3, no degradation of the properties is observed. On the other hand, for Fe_2O_3 contents greater than 200 p.p.m, ε and Qf decrease drastically, due to the decrease in bulk density.

3.1.6. Conclusion

$(BaO)_{0.15}(Sm_2O_3)_{0.15}(TiO_2)_{0.7}$ composition leads effectively after sintering to microwave characteristics easily optimizable by a control of the calcination and sintering processes. Moreover, addition of Fe_2O_3 in small quantities as a dopant can completely eliminate the porosity. However, whatever the sintering schedule, secondary phases $Ba_2Ti_9O_{20}$ and TiO_2 are present. The amounts of these secondary phases are not easily controlled. The presence of TiO_2 which has a large τf(τf = + 427 p.p.m.) even in a low quantity, may lead to reproductibility problems and may influence microwave characteristics.

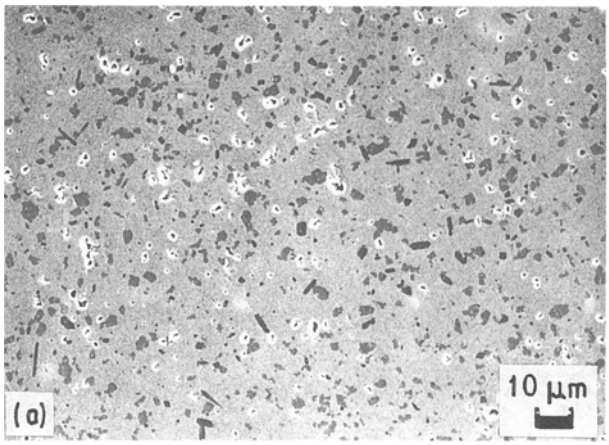

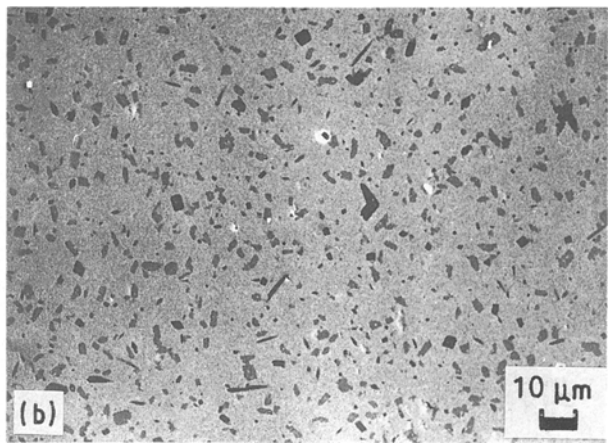

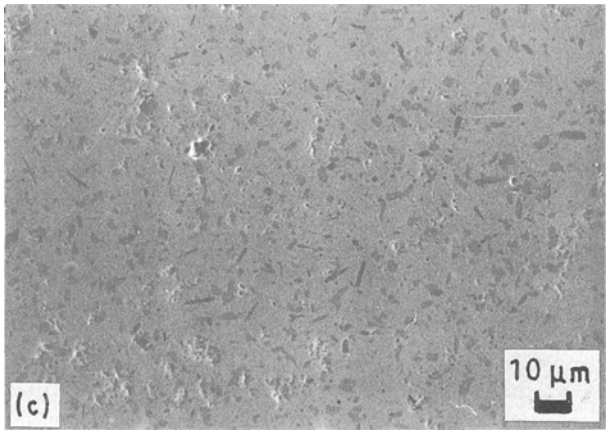

Figure 6 Polished surface of composition 'a' samples sintered at 1350 °C in the presence of different Fe_2O_3 ratios (a) no dopant, (b) 200 p.p.m. Fe_2O_3, (c) 300 p.p.m. Fe_2O_3.

TABLE IV Microwave characteristics and density evolution versus sintering temperature of composition 'a' (calcination at 950°C)

Sintering temperature (°C)	Density	ε	Qf(GHz)	τf(p.p.m. °C^{-1})
1350	5.59	75	8800	− 3
1360	5.44	72	8300	+ 4
1370	5.44	72	8200	+ 4

TABLE V Microwave properties of composition 'a' versus Fe_2O_3 content after sintering at 1350 °C for 2 h in an oxygen atmosphere

Fe_2O_3 amount (p.p.m.)	Density	ε	Qf(GHz)	τf(p.p.m. °C^{-1})
0	5.59	78	8900	− 6
100	5.6	77.6	8140	− 6
200	5.6	77	8200	− 6
300	5.56	74	4900	− 7.5

Thus it is of interest to explore other compositions as close as possible to the theoretical homogeneity range of the bronzoid $Ba_{6-x}Sm_{8+2x/3}Ti_{18}O_{54}$ in order to limit the formation of secondary phases and, in particular, TiO_2. The elimination of TiO_2 should allow the τf coefficient to be decreased. Such compositions, if they exist, should allow, by mixing rule applications, or by partial replacement of samarium by neodymium, low τf conciliation of low values (near zero) with a reasonably high dielectric constant (close to 80).

3.2. Exploration of new compositions for the bronzoid $Ba_{6-x}Sm_{8+2x/3}Ti_{18}O_{54}$

In order to determine the influence of the presence of the secondary phase upon microwave properties, we have studied several compositions, intermediate between composition 'a' and the theoretical line AB which characterizes the pure bronzoid $Ba_{6-x}Sm_{8+2x/3}Ti_{18}O_{54}$ (Fig. 1). In addition to these different compositions, b–k, two other compositions, l and m, have also been sintered. Note also that compositions h, k, l have been studied previously [8–10].

3.2.1. Existence of a single-phase domain

As for composition 'a', one does not observe any mixture by XRD after sintering. Whatever the composition, the diffractogram is characteristic of the pure bronzoid. However, this result cannot be considered as a purity criterion, because $Ba_2Ti_9O_{20}$ and TiO_2 phases, if they are present, are in very small amounts and their diffraction peaks overlap with those of the bronzoid.

The systematic SEM observations are more sensitive to the presence of secondary phases. The different microstructures are shown in Fig. 7, and the phases which are observed for different compositions are given in Table VI. Composition l, which was chosen as a reference for increasing the TiO_2 content, corresponds as expected, to a mixture, which exhibits besides the main bronzoid phase, secondary phases TiO_2 and $Ba_2Ti_9O_{20}$ in significant amounts.

One important feature is that other compositions except composition m, have only one secondary phase and that the amount of secondary phase decreases when approaching the bronzoid line AB. For a constant amount of barium in the mixture, i.e. going from d → g → k, one observes only one secondary phase whose content decreases. From the peudo ternary diagram (Fig. 1) one can postulate either the presence of TiO_2 or the presence of barium titanate. No peak appears in the X-ray diffraction pattern; only the EDS

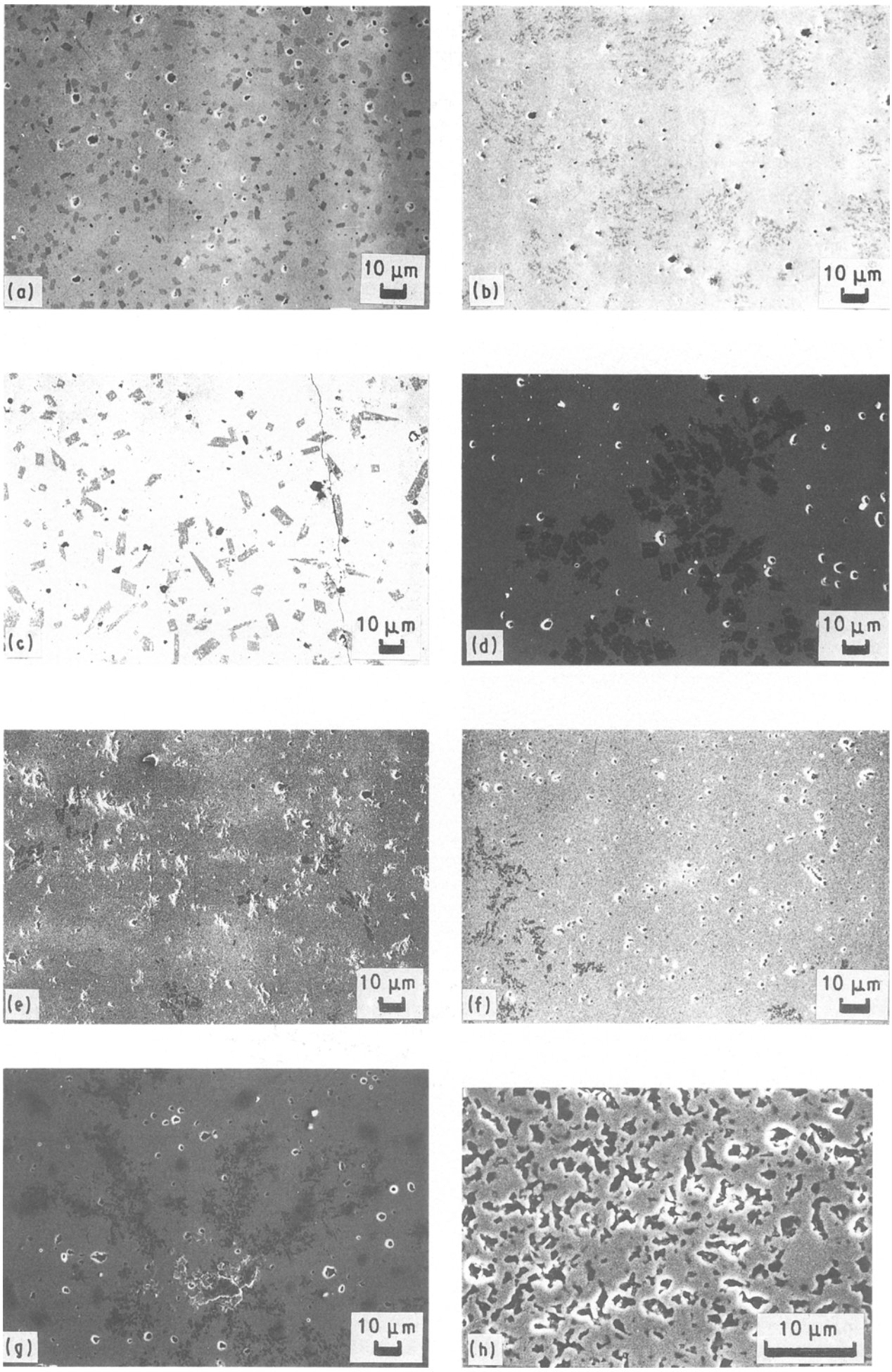

Figure 7 Microstructure evolution of samples sintered at 1350 °C versus composition: (a – m) refer to a – m on ternary diagram in Fig. 1.

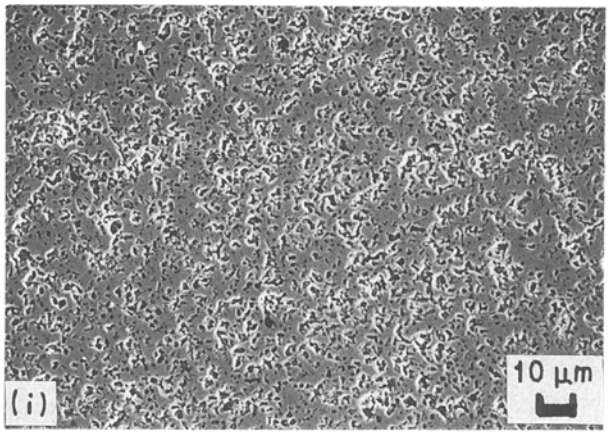

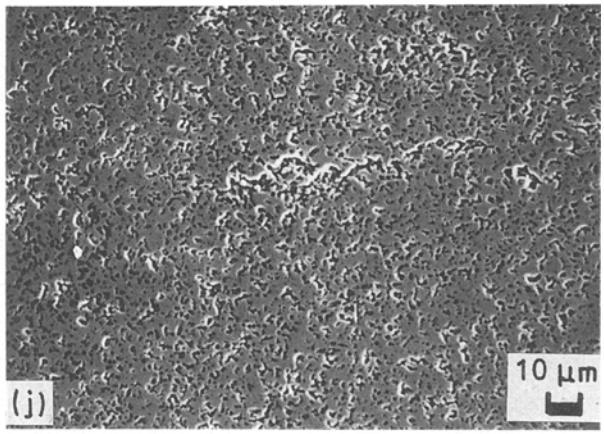

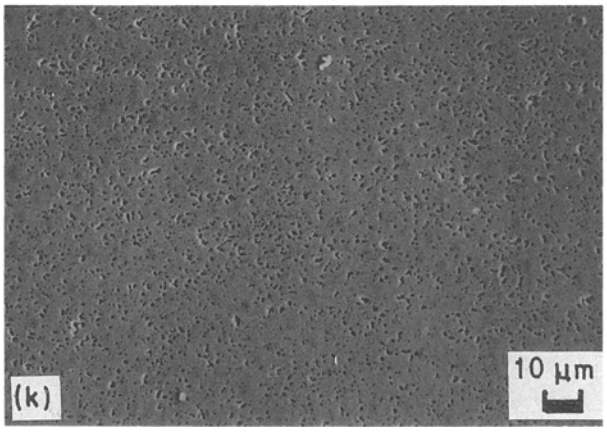

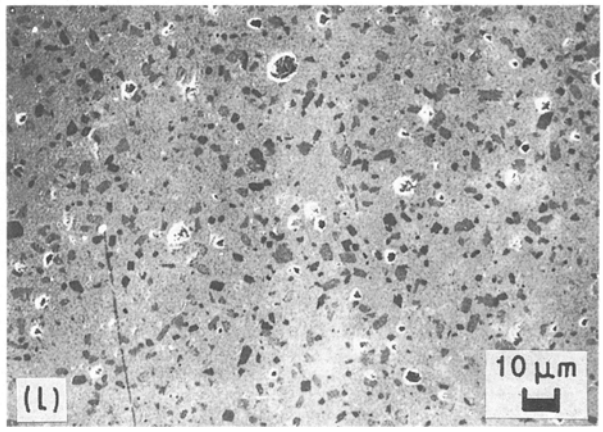

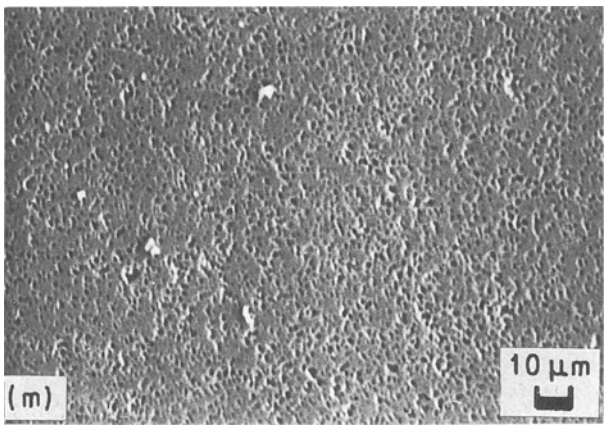

Figure 7 continued

analysis can indicate the nature of the secondary phase. This analysis indicates that the secondary phase is probably $Ba_2Ti_9O_{20}$. The subsisting doubt is due to the great difficulty in preparing pure barium titanate $Ba_2Ti_9O_{20}$ as a reference, in particular because of the existence of several titanates with different Ti/Ba ratios close to each other.

A similar evolution is observed along the lines e, f, g and b, e, i; in the latter line the evolution is less evident owing to the fact that the excess $Ba_2Ti_9O_{29}$ is much lower.

The second important feature concerns the existence of a pure phase not only for the pure bronzoid line AB, but also for compositions i and m according to SEM observations. In the same manner, composition e contains very small amounts of secondary phases. However, such secondary phases might be hidden by the large porosity of the materials especially for samples i and m. Another possibility is the formation of an amorphous phase. A final hypothesis would be that the homogeneity range of the bronzoid phase extends outside the ideal line AB; the close relationships between the bronzoid, perovskite and tetragonal tungsten bronze structures is in agreement with this view point, because it suggests the possible formation of intergrowth between these structures [11].

3.2.2. Densification

The micrographs of the different compositions a to m (Fig. 7), show that pure phases are characterized by a poor densification, contrary to those containing TiO_2 or $Ba_2Ti_9O_{20}$ which are well densified. It is also clear that porosity increases as the TiO_2 content decreases. This confirms that TiO_2 acts as a sintering agent, in agreement with the mechanism described by Yan and Johnson [12] to explain the interdiffusion phenomena between TiO_2 and magnesium zinc ferrites leading to a discontinuous grain growth.

In order to confirm the role of TiO_2 as a sintering agent we have realized an interface between a TiO_2 disc and a disc of composition i. The pressed sample was sintered at 1350°C for 2 h. A large increase in porosity was observed when moving away from the interface in disc i. The role of the sintering agent of TiO_2 is also confirmed by evolution of the microstructure of the ceramic (Fig. 8) which exhibits lower grains near the interface.

TABLE VI Microstructures and microwave properties versus composition for to the (BaO) (Sm_2O_3) (TiO_2) ternary diagram. For key to letters, see Fig. 1.

Composition		Sintering temperature (°C)	Density	ε	Qf (GHz)	τf (p.p.m. °C^{-1})	SEM observation
(a)	$BaSm_2Ti_{4.67}O_{13.34}$	1350	5.50	77	9000	± 3	ϕ + TiO_2(s) + $Ba_2Ti_9O_{20}$(s) + porosity (m)
(b)	$BaSm_{2.13}Ti_{4.46}O_{13.13}$	1350	5.64	78	8200	0	ϕ + porosity (m) + $Ba_2Ti_9O_{20}$ (m)
(c)	$BaSm_{1.93}Ti_{4.2}O_{12}$	1350	5.54	78	8200	− 5	ϕ + $Ba_2Ti_9O_{20}$(s) + porosity (m)
(d)	$BaSm_{1.73}Ti_{3.93}O_{11.4}$	1350	5.62	78	5000	− 2	ϕ + $Ba_2Ti_9O_{20}$(s) + porosity (w)
(e)	$BaSm_2Ti_{4.53}O_{13.34}$	1350	5.65	81	8500	− 7 − 11	ϕ + $Ba_2Ti_9O_{20}$(s) + porosity (w)
		1350	5.69	81	8300	− 17	ϕ + $Ba_2Ti_9O_{20}$(s) + porosity (w)
		1380	5.68	82	6200	− 2	ϕ + $Ba_2Ti_9O_{20}$(s) + porosity (w)
(f)	$BaSm_{2.13}Ti_{4.13}O_{12.26}$	1350	5.65	81	7600	− 8	ϕ + $Ba_2Ti_9O_{20}$(s) + porosity (w)
(g)	$BaSm_{1.8}Ti_{3.86}O_{11.4}$	1350	5.63	82	4900	− 3	ϕ + $Ba_2Ti_9O_{20}$(s) + porosity (w)
(h)	$BaSm_{2.53}Ti_{4.8}O_{14.4}$	1350	3.89	40	4500	+ 11	ϕ + porosity (s)
(i)	$BaSm_{2.3}Ti_{4.38}O_{13.2}$	1350	4.85	61	4600	− 8.3	ϕ + porosity (s)
		1380	5.40	75	4500	− 4.7	ϕ + porosity (m)
(j)	$BaSm_{2.06}Ti_{4.06}O_{12.29}$	1350		Not	measurable		ϕ + porosity (s)
(k)	$BaSm_{1.86}Ti_{3.8}O_{11.4}$	1350	5.34	74		− 3	ϕ + porosity (s)
(l)	$BaSm_2Ti_5O_{14}$	1350	5.45	77	9300	+ 12	ϕ + TiO_2(s) + $Ba_2Ti_9O_{20}$ (m) + porosity (m)
(m)	$BaSm_{2.5}Ti_{4.5}O_{13.75}$	1350	4.7	56	3100	+ 21	ϕ + porosity (s)
		1380	5.28	70	3400	+ 15	ϕ + porosity (m)
		1430	5.64	76	2800	+ 9.7	ϕ + porosity (w)
		1460	5.68	78		+ 8	ϕ + porosity (w)

ϕ, Bronzoid matrix; (m), medium; (w), weak; (s), strong.

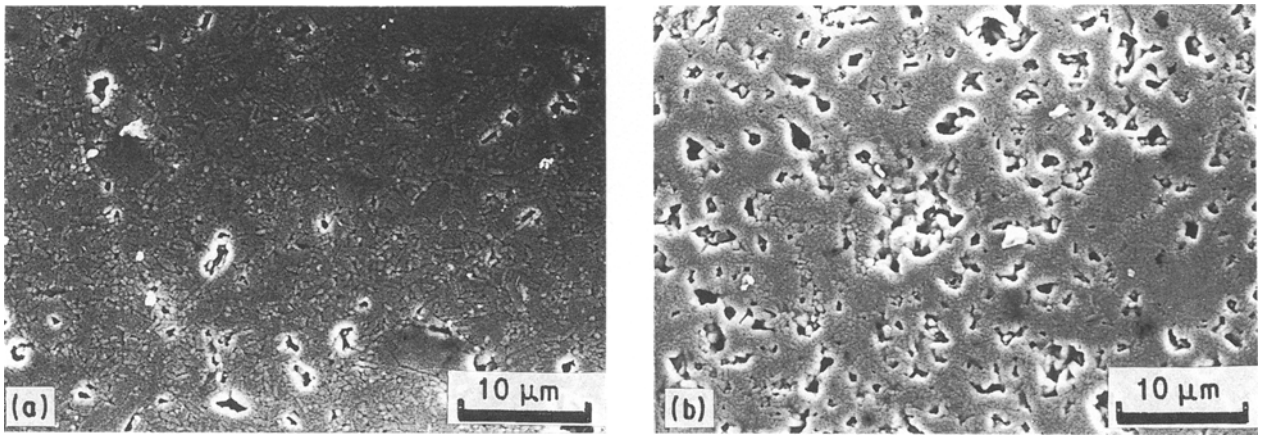

Figure 8 TiO_2 influence on densification of a ceramic sintered at 1350 °C (composition i): (a) close to the interface, (b) far away from the interface zone.

3.2.3. Microwave properties versus composition

The microwave properties for the different compositions sintered at various temperatures, and tested at 3 GHz are listed in Table VI. ε is seen to increase slightly when moving towards the bronzoid line, in spite of decreasing the TiO_2 content, i.e. along the lines abe, cf and dg, respectively. However, a dramatic decrease of the dielectric constant is observed for the compositions belonging to the bronzoid line AB. This phenomenon is easily explained by the poor densification of these compositions (j k) at 1350 °C. In the same way, the results obtained for samples i and m, at various sintering temperatures show that ε is closely related to the densification degree.

The variation of Qf factor is more difficult to interpret. For poorly densified samples (j and k), Qf is not measurable. However, one generally observes a decrease in Qf when moving towards the pure bronzoid line. This is illustrated by the line l, a, b, e (Table VI)

which shows a progressive decrease of Qf from 9300 GHz for composition 1 to 8500 GHz for composition e. From Q values of $Ba_2Ti_9O_{20}$ and TiO_2, 10 000 and 14 600 at 3 GHz, respectively [6], (i.e. Qf 30 000 and 43 800 GHz), one should obtain a lower Qf factor for the well-densified pure bronzoid than for sample 'a' if one postulates that the Qf value is related to the amount of each secondary phase.

In a general manner, τf decreases slowly when moving towards the bronzoid line. However, the τf value for a given composition seems to be closely related to the sintering cycle (temperature, time, etc.). Moreover, for a given composition and a given sintering cycle, fluctuations of τf are sometimes observed. This phenomenon is all the more accentuated for compositions which are close to the pure bronzoid line (see, for instance, compositions e and m, Table VI). It is worth pointing out that negative τf values can be obtained when going towards the line AB, as shown for sample e (-17 p.p.m. $°C^{-1}$) and samples f and i (-8 p.p.m. °C). Nevertheless, the τf value of -30 p.p.m. $°C^{-1}$, postulated by Wu and Chang [6] for an hypothetical single phase has not been reached. This can be explained by the fact that the sintering process of the single phase has not yet been optimized. Moreover, the -30 p.p.m. $°C^{-1}$ τf value postulated previously [6] does not take into account the large homogeneity range of the bronzoid, i.e. the possible variation of τf along the line AB (Fig. 1). Thus, if one takes into account the microstructure and the microwave properties, composition e appears to be the best compromise when sintered at 1350 °C.

4. Conclusion

This study shows that the single-phase compositions, corresponding to the homogeneity range $Ba_{6-x}Sm_{8+2x/3}Ti_{18}O_{54}$, are potential materials for microwave applications, although their sintering process has not yet been optimized. Moreover, a homogeneity range is susceptible to exist outside the bronzoid line. There is no doubt that the pure bronzoid will lead to negative τf value, which can be greatly modulable by substitutions on the barium and samarium sites. In this respect, composition e appears to be the most promising, because its dielectric constant and loss angle are in good agreement for use as microwave resonators in the range 1–3 GHz. The main area of improvement of these properties lies in the densification of this composition; a study of this is in progress.

Acknowledgements

This work was performed in collaboration with the Tekelec Composants company (Tekelec Composants, Parc Industriel Bersol 33600 Pessac, France) and supported by the DAII (French Telecom: Direction des Affaires Industrielles et Internationales, Contract no 8935/23).

References

1. S. NISHIGAKI, H. KATO, S. YANO and R. KAMIMURA, *Ceram. Bull.* **66** (1987) 9.
2. D. KOLAR, Z. STADLER, S. GABERSCEK and D. SUVOROV, *Ber. Dr. Keram. Ges.* **55** (1978) 7.
3. K. WAKINO, K. MINAI and H. TAMURA, *J. Amer. Ceram. Soc.* **67** (1984) 278.
4. M. B. VARFOLOMEEV, A. S. MIRONOV, V. S. KOSTOMAROV, L. A. GOLUBTSOVA and T. A. ZOLOTOVA, *Russ. J. Inorgan. Chem.* **33** (1988) 4.
5. S. W. HAKKI and P. D. COLEMAN, I.R.E. Transactions on Microwave Theory and Techniques (1960) pp. 402–410.
6. J. M. WU and M. C. CHANG, *Amer. Ceram. Soc.* **73** (1990) 1599.
7. H. M. O'BRIAN and J. THOMSON, *J. Amer. Ceram. Soc.* **57** (1974) 522.
8. R. G. MATVEEVA, M. B. VARFOLOMEEV and L. S. LL'YUSHCHENKO, *Russ. J. Inorgan. Chem.* **29** (1984) 17.
9. D. KOLAR, *J. Solid State Chem.* **38** (1981) 158.
10. T. JAAKOLA, A. UUSIMAKI, R. RAUTIOAHO and S. LEPPAVUORI, *J. Amer. Ceram. Soc.* **69** (1986) C234.
11. V. A. ISUPOV, *Ferroelectric* **76** (1987) 107.
12. M. F. YAN and D. W. JOHNSON Jr, *J. Amer. Ceram. Soc.* **61** (1978) 342.

Received 6 June
and accepted 22 October 1991